Earth and Planetary Science Letters 584 (2022) 117426

Contents lists available at ScienceDirect

Earth and Planetary Science Letters

www.elsevier.com/locate/epsl

The tectonic context of hafnium isotopes in zircon

K.E. Sundell [a,*], F.A. Macdonald [b]

[a] Department of Geosciences, Idaho State University, Pocatello, ID, USA
[b] Department of Earth Science, University of California, Santa Barbara, Santa Barbara, CA, USA

ARTICLE INFO

Article history:
Received 20 June 2021
Received in revised form 6 January 2022
Accepted 7 February 2022
Available online xxxx
Editor: A. Webb

Keywords:
supercontinent
plate tectonics
zircon
hafnium
orogenesis

ABSTRACT

The assembly and dispersion of continental crust are first-order controls on paleogeography and geochemical cycles. The associated reworking of Earth's crust can be tracked with zircon initial hafnium (εHf_T) through space and time. Here we apply a new method of quantitative analysis using εHf_T density estimates based on a compilation of 155,329 εHf_T values. Investigation of the global database reveals significant geographic and temporal bias in the εHf_T record associated with sampling and regional tectonic events. Recent research has attempted to address global εHf_T bias using resampling methods to augment gaps of low εHf_T data density, which in turn obfuscates tectonic signals and artificially weights outliers. Instead, we evaluate εHf_T density patterns for both igneous and detrital zircon on eight continental zones demarcated by Paleozoic sutures: Africa, Antarctica, Asia, Australia, Baltica, North America, Peri-Gondwana, and South America. Pairwise two-dimensional quantitative comparison highlights similarity in timing and εHf_T values between zones, all of which can be linked to documented shared regional tectonism. Integration of all pairwise comparisons reveals that peak similarity corresponds to the timing of supercontinent amalgamation, and that the associated εHf_T differs depending on the style of supercontinent amalgamation, particularly internal versus external orogenesis. The three most recent supercontinents produced distinctive εHf_T signals, shared by the constituent continental zones. The supercontinents Rodinia and Pangea were constructed through collisions of marginal arc terranes, peripheral to ancient crust, and did not produce highly enriched εHf_T values. In contrast, Ediacaran to Cambrian formation of the Gondwana supercontinent was largely the product of internal Pan-African orogens that formed directly after Neoproterozoic Rodinia rifting and arc accretion forming the Arabian Shield. The final assembly of Gondwana was dominated by continent-continent collisions of old radiogenic crust without establishment and accretion of extensive intervening depleted arc terranes, resulting in a more enriched distribution of εHf_T values compared to prior and subsequent supercontinent formation. The secular εHf_T record is the product of spatiotemporally biased sampling and preservation of specific orogenic belts with predictable εHf_T data arrays, modulated by the amalgamation, tenure, and breakup of supercontinents through time.

1. Introduction

Zircon is a geochemical time capsule of the Earth's crust. Because it is physically and chemically robust and undergoes little post-crystallization diffusion, it can survive multiple tectonic cycles. Critical for geochronology, zircon contains abundant U and Pb with small amounts of common Pb upon crystallization (Schoene, 2014). Additionally, for petrogenesis, the Hf systematics (i.e., radiogenic versus non-radiogenic) depend on the amount of mantle-derived material relative to older crust incorporated in the melt. Because Hf is charge bound and in high concentration relative to Lu, the initial Lu-Hf ratio at the time of crystallization in zircon (εHf_T) undergoes little change once formed (Vervoort and Blichert-Toft, 1999).

Patterns in global compilations of zircon εHf_T have been interpreted to record wholesale modulations in Earth processes, including changes in crustal growth and reworking (i.e., remobilization within the crust) (Belousova et al., 2010; Condie et al., 2011; Dhuime et al., 2012; Roberts and Spencer, 2015), the onset and style of plate tectonics (Sobolev and Brown, 2019), enhanced erosion associated with Snowball Earth glaciations (Keller et al., 2019), supercontinent amalgamation and breakup (*e.g.*, Collins et al., 2011; Roberts and Spencer, 2015), and the earliest formation of continental crust (*e.g.*, Dhuime et al., 2012). Positive and negative excursions in global records of εHf_T relative to the depleted mantle (Earth's upper mantle depleted in incompatible elements)

* Corresponding author.
E-mail address: kurtsundell@isu.edu (K.E. Sundell).

https://doi.org/10.1016/j.epsl.2022.117426
0012-821X/

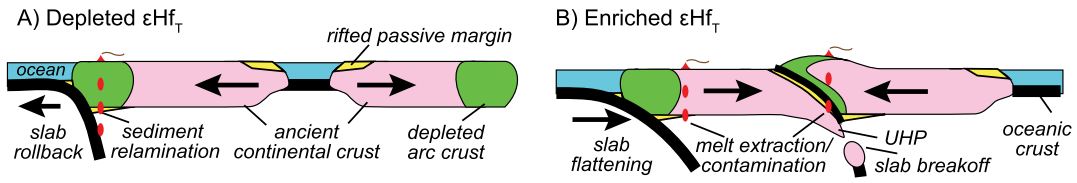

Fig. 1. The tectonic context of hafnium in zircon wherein tectonic setting controls melt εHf_T. A) Zircon with depleted εHf_T forms from subduction melt on oceanic crust or young continental crust, or from rifting of young continental crust. B) Zircon with enriched εHf_T is produced by melt extraction of old crustal material subduction of ocean or continental crust, or during subduction sediment from a former passive margin containing old detrital zircon. UHP = ultra-high pressure.

can be used to interpret regional orogenic events in a predictable plate tectonic context modulated by supercontinent amalgamation and separation. In this context, supercontinent formation can be deconstructed as a series of orogens between a set of converging continents and intervening terranes. Thus, records of zircon εHf_T values through supercontinent formation and dispersal may depend on the orogenic styles (*e.g.*, Collins et al., 2011), composition of colliding terranes (Spencer et al., 2013), and completeness of sampling. Although previous work has recognized opposing εHf_T and seawater Sr isotope trends through different supercontinent tenures (Spencer et al., 2013), the tectonic context of εHf_T through time (i.e., regional tectonic setting, crust and mantle components involved in melting, and type of orogenesis as a control on εHf_T) has not been generalized and has opened up alternative interpretations such as an outsized role of glacial erosion (Keller et al., 2019) or secular changes in plate tectonics (Sobolev and Brown, 2019).

Data interpretation methods have been developed specifically for interpretation of εHf_T (*e.g.*, Andersen et al., 2018), but have generally lacked geographic metadata (i.e., sample locations) critical to assessing interpretation bias. For example, interpretations of global phenomena have been made based on calculation of εHf_T running averages (*e.g.*, Roberts and Spencer, 2015), modeling of mantle extraction ages to determine the amount of mantle-derived additions to the Earth's crust through time (Belousova et al., 2010), and resampling inversely to data density in attempt to augment low density gaps in the global record (Keller et al., 2019). We use a new two-dimensional quantitative method (Sundell and Saylor, 2021) to compare bivariate kernel density estimates (KDEs) based on a recent global compilation of both igneous and detrital zircon εHf_T data (Puetz et al., 2021) separated geographically based on preserved Paleozoic sutures. The new method provides a time-resolved measure of εHf_T similarity between datasets and allows for incorporation of geographic context. In this framework, we test whether trends in the εHf_T global database correspond to global Earth processes, or rather if they result from specific orogenic events that bias the εHf_T record at different times associated with supercontinent formation and dispersal.

2. Hafnium isotopes in zircon

Different tectonic settings have predictable zircon εHf_T values based on the relative proportion of depleted mantle to older continental crust involved in melting. Melting of the mantle results in the loss of incompatible trace elements to the melt and subsequent transfer to the crust, leaving Earth's upper mantle relatively depleted (Hofmann, 1997). Because zircon is a primary sink for Hf in continental crust (Bea, 1996), it is a proxy for how much isotopically depleted (i.e., radiogenic, depleted mantle material) versus isotopically enriched (i.e., nonradiogenic, older crustal material) was incorporated in the host melt in which it grew. Oceanic arcs and continental arcs formed on young crust will produce isotopically depleted (more positive) εHf_T in zircon (Fig. 1A) with εHf_T values that plot close to the depleted mantle, similar to those formed in ocean island arc basalts in the modern Andes (Pepper et al., 2016). Melting of continental crust and incorporation of old zircon will produce isotopically enriched εHf_T in younger zircon that deviates towards more negative values from the depleted mantle line. There are two primary ways to produce zircon with enriched εHf_T. The first is to 'contaminate' melt by partially melting older continental crust via melt extraction during subduction beneath old, thickened continental crust (Fig. 1B), such as in the Laramide orogen in the northern U.S. (Stevens et al., 2016); this includes melt extracted from high temperature granulites and migmatites. The second is to subduct and melt crust containing abundant old detrital zircon from the lower plate (Fig. 1B), as happens when a formerly rifted passive margin and underlying continental crust is subducted (Patchett et al., 1984). During arc-continent and continent-continent collisions, these two processes occur in a continuum as melt is extracted both from subducted sediment, the underlying continental crust, and the thickened upper plate. The range of zircon εHf_T values depends critically on the εHf_T of the colliding plates and the amount of isotopically depleted material between them. For example, a recipe for creating a dense array of negative εHf_T values is a collision between two Paleoproterozoic or older continental margins with minimal isotopically depleted arc material (i.e., a narrow ocean basin) between them.

3. Methods

3.1. Hafnium isotope data and database treatment

We interrogate a recent compilation of igneous and detrital zircon εHf_T data (Puetz et al., 2021). Hf isotope geochemical data are reported in ε units in reference to the chondritic uniform reservoir (CHUR), expressed as:

$$\varepsilon Hf_T = \left(\frac{\frac{176Hf}{177Hf} - \frac{176Lu}{177Hf} \times e^{\lambda T - 1}}{C_{Hf,CHUR(0)} - C_{Lu,CHUR(0)} \times e^{\lambda T - 1}} - 1 \right) \times 10{,}000.$$

Here, T is the zircon crystallization date produced via U–Th–Pb geochronology (*e.g.*, Schoene, 2014), $^{176}Hf/^{177}Hf$ and $^{176}Lu/^{177}Hf$ are the measured isotopic values within zircon, λ is the ^{176}Lu β-decay rate of 1.867×10^{-5}/Myr (Söderlund et al., 2004), $C_{Hf,CHUR(0)}$ and $C_{Lu,CHUR(0)}$ are present day $^{176}Hf/^{177}Hf$ and $^{176}Lu/^{177}Hf$ for CHUR of 0.282772 and 0.0332 (Griffin et al., 2000). The depleted mantle array is calculated using an initial $^{176}Hf/^{177}Hf$ value of 0.283225 and initial $^{176}Lu/^{177}Hf$ value of 0.0383 (Vervoort and Blichert-Toft, 1999). Average crustal evolution trends assume modern $^{176}Lu/^{177}Hf$. Calculation of εHf_T results in a value representing parts per 10,000 deviation from the CHUR at the time of zircon crystallization.

The εHf_T data was subdivided along Paleozoic terrane boundaries of Domeier and Torsvik (2014) to produce eight zones: Africa, Antarctica, Asia, Australia, Baltica, North America, Peri-Gondwana, and South America (Fig. 2A). Africa includes the broader Arabian Peninsula with data from Israel, Oman, and Saudia Arabia. Asia is separated from Peri-Gondwanan terranes along the Paleo-Tethys suture between Peri-Gondwana and peri-Eurasian terranes (Metcalfe, 2013) and includes the Siberian, Tarim, North China, South China cratons and terranes in the Central Asian Orogenic Belt. Australia includes the SE Asian terranes that were situated on the

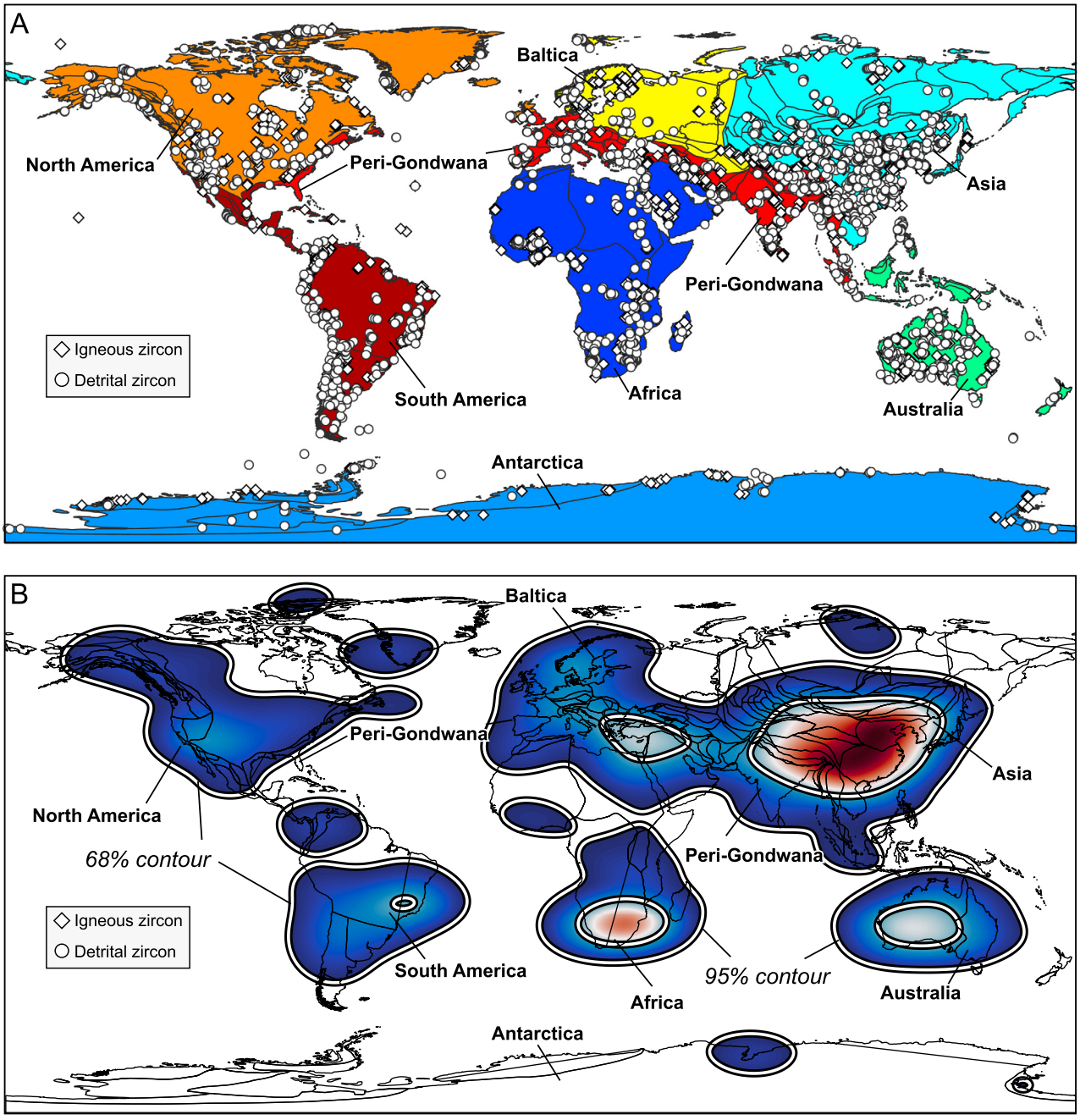

Fig. 2. Global distribution of εHf_T data. A) Map showing global distribution of εHf_T data and continental zones for this study. Paleozoic sutures are from Domeier and Torsvik (2014). B) Bivariate KDE of data density in part A using 10° and 5° kernel bandwidths in the longitude and latitude directions, respectively.

southern margin the Meso-Tethys prior to the Jurassic (Metcalfe, 2013). Baltica and Asia are separated from Peri-Gondwanan terranes along the Paleo-Tethys suture (Domeier and Torsvik, 2014) and separated from Asia along the eastern flank of the Ural Mountains. North America is separated from Peri-Gondwanan terranes along the Iapetan suture (Domeier and Torsvik, 2014). Peri-Gondwana includes terranes along the North American eastern seaboard from Suwannee (Florida) to Avalonia (Atlantic Canada); European terranes south of Scandanavia and the Ukrainian Shield; the central and south Pamir; the Qiangtang, Lhasa, and Tethyan Himalayan terranes of the Hima-Tibetan plateau; India; and terranes west of south China and Java. South America includes terranes of Mexico and Central America.

Next, the subdivided database was binned into 100 Myr intervals for each of the zones and separated into igneous and detrital zircon data to determine their cumulative percent contribution through time (Fig. 3A–B). The database was further subdivided based on deviation from depleted mantle for igneous and detrital zircon data from each continental zone (Fig. 3C–R). The difference in $^{176}Hf/^{177}Hf$ between the depleted mantle and continental crust increases with time. As such, εHf_T data were separated into four groups with "depleted" values within 10 ε units negative deviation from depleted mantle, "slightly enriched" values between 10 and 20 ε units negative deviation from depleted mantle, "enriched" values between ε units 20 and 30 negative deviation from depleted mantle, and "highly enriched" values >30 ε units negative deviation from depleted mantle.

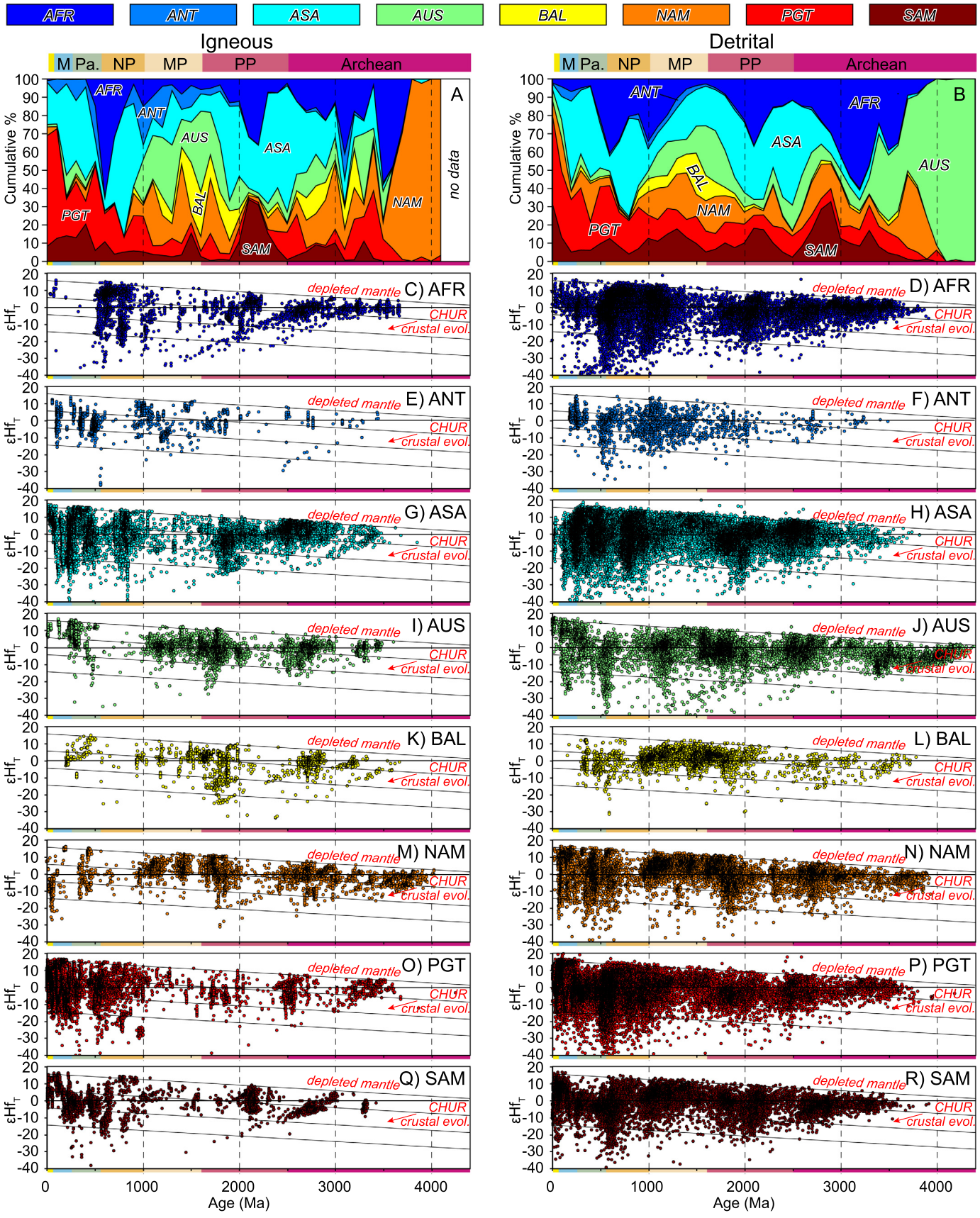
AFR
ANT
ASA
AUS
BAL
NAM
PGT
SAM
Igneous
Detrital
M Pa.
NP
MP
PP
Archean
A
B
Cumulative %
no data
C) AFR
D) AFR
E) ANT
F) ANT
G) ASA
H) ASA
I) AUS
J) AUS
K) BAL
L) BAL
M) NAM
N) NAM
O) PGT
P) PGT
Q) SAM
R) SAM
depleted mantle
CHUR
crustal evol.
εHf_T
Age (Ma)

3.2. Data visualization

Bivariate KDEs are an objective way to evaluate εHf_T data by providing an assessment of data density that takes into account both age and zircon chemistry (*e.g.*, Andersen, 2014; Roberts and Spencer, 2015; Spencer et al., 2019; Sundell et al., 2019). Bivariate KDEs were generated using modified MATLAB code from *DZstats-2D* and *HafniumPlotter* (Sundell et al., 2019; Sundell and Saylor, 2021). The routine generates bivariate KDEs by performing a discrete cosine transform of the discrete data (Ahmed et al., 1974), multiplying the resulting matrix by a Gaussian function with set kernel bandwidths in the x and y directions, performing an inverse discrete cosine transform of the Gaussian-scaled matrix, and normalizing the resulting three-dimensional volume to one.

Bivariate KDEs are visualized as color-coded intensity plots in two-dimensional (2D) space (i.e., parallel to the z-axis) using a perceptually uniform *cmocean* 'balance' color map from Thyng et al. (2016) so that the data may be perceived without artificial weighting. For consistency, and to aid interpretation of density modes, all density plots are clipped at 95% from peak density (i.e., the lowest 5% density is shown as white space). Bivariate KDEs were generated for the eight continental zones listed above over 4400 and 0 Ma with kernel bandwidths of 20 Myr and 1 ε units (Fig. 4). Geographic contribution of εHf_T to the global database was also characterized using a bivariate KDE, constructed based on longitude-latitude locations using a 10° bandwidth in the x-axis (longitude) and a 5° bandwidth in the y-axis (latitude), which represents ~3% distance in each direction on an equal area projection of Earth (Fig. 2B).

3.3. Quantitative comparison and the similarity sum

Bivariate KDEs of the eight continental zones were quantitatively compared following the '2D similarity' technique outlined in Sundell and Saylor (2021). Here, the geometric mean is calculated sequentially for all points bound within the x-axis and y-axis of two bivariate KDEs. The 2D similarity method is a simple mathematical extension of the *Bhattacharyya Coefficient* between two discrete probability distributions in one dimension (Bhattacharyya, 1943). The resulting matrix from comparing two bivariate KDEs is summed to produce a single value, S, between 0 and 1:

$$S = \sum_{i,j=1}^{i,j=n} \sqrt{f(i,j) \times g(i,j)}$$

where f and g are matrices of z-axis values that share common $i \times j$ discrete points on a square grid. A useful way to visualize similarity is to plot the 'intermediate step' of calculating S where the geometric mean of each pair x–y grid points is calculated, but not summed. The resulting matrix can be shown as a standard bivariate KDE that highlights where the compared distributions are similar. We apply this method in a pairwise manner for the eight continental zones, which produces twenty-eight comparisons (Fig. 5). Results are compared to simplified paleogeographic reconstructions of supercontinents (Fig. 6), then summed into a single bivariate KDE as a test of when εHf_T similarity occurs in the global record (Fig. 7).

4. Results

Contributions to the global εHf_T database are summarized in Figs. 2–4 and in Table 1 and for the eight continental zones of Africa, Antarctica, Asia, Australia, Baltica, North America, Peri-Gondwana, and South America. Geographic data density is concentrated in two locations globally, Asia and southern Africa (Fig. 2B). Igneous zircon data make up 30% of the database, whereas detrital zircon data contribute 70% (Table 1). In all cases except for Antarctica, detrital data contributions are higher than igneous data, and in most cases detrital data make up two to three times the overall contribution; Africa detrital data contribute more than four times as much as igneous data (Table 1). Individual zones show starkly different overall contributions to the zircon εHf_T database. For example, Asia and Peri-Gondwana have the highest contributions at 28% and 20%, whereas Baltica and Antarctica have the lowest contributions at ~3%; all other continental zones contribute roughly 10% and 20% of data to the database (Table 1).

Contributions to the global εHf_T database vary in space and time (Fig. 3A–B). Binning the database into 100 Myr intervals to calculate cumulative percent contribution of each continental zone through time shows that the database is dominated by different zones over particular intervals. The Hadean (>4000 Ma) is dominated by Australia, whereas the Archean (4000–2500 Ma) is dominated by Africa, Australia, and North America (Fig. 3A–B). The Paleoproterozoic and Mesoproterozoic (2500–1000 Ma) are initially dominated by Asia and Africa, with increasing contributions of other continental zones through time (Fig. 3A–B). At ~1500 Ma, the populations are as close to being equal as in any time in Earth's history (excluding Antarctica), which shifts dramatically to a dominance by Africa, Asia, Peri-Gondwana, and South America during the Neoproterozoic (1000–541 Ma) (Fig. 3A–B). Asia, Peri-Gondwana, and South America data compose the overwhelming majority of the Phanerozoic (541–0 Ma). Antarctica and Baltica are never major contributors to the global database (Fig. 3A–B).

Database contributions parsed by Hf systematics (i.e., negative deviation from depleted mantle) reveal markedly variable results (Fig. 3B–R and Table 1). The global εHf_T database comprises 46% depleted εHf_T (within 10 ε of depleted mantle), 40% slightly enriched εHf_T (between 10 and 20 ε of depleted mantle), 12% enriched (between 20 and 30 ε of depleted mantle), and only 3% highly enriched (> 30 ε negative deviation from depleted mantle) for all of Earth time (Table 1).

The detrital εHf_T signal shows more dispersion at different time intervals than the igneous εHf_T record (compare left and right columns in Fig. 3C–R). All eight continental zones show crustal evolution trends (i.e., a decreasing array of εHf_T through time); however, some are more prominent (i.e., linear and roughly continuous) than others, particularly in the igneous data compilations, such as the Archean to Mesoproterozoic Africa (Fig. 3C) and South America (Fig. 3Q).

Bivariate KDEs reveal density modes from clusters of εHf_T data for the continental zones Fig. 4). The earliest εHf_T density modes are depleted to slightly enriched in the Neoarchean (2800–2500 Ma) in North America and South America (Fig. 4F,H), followed by a depleted mode in Asia at ~2500 Ma (Fig. 4C). Australia, Baltica and North America have depleted to slightly enriched modes between 2000 and 1500 Ma (Fig. 4D–F). North America shows two depleted modes between 1600 and 1000 Ma (Fig. 4F). The late Neoproterozoic shows depleted to enriched modes in Africa, Antarctica, Peri-

Fig. 3. Geographic and temporal distribution of εHf_T data by continental zone and Hf systematics. Cumulative percent contribution of εHf_T for A) igneous zircon and B) detrital zircon. AFR = Africa. ANT = Antarctica. ASA = Asia. AUS = Australia. BAL = Baltica. NAM = North America. PGT = Peri-Gondwana. SAM = South America. C–R) εHf_T data separated into igneous (left column) and detrital (right column) contributions to the global database, each show four groups based on Hf systematics are "depleted" values within 10 ε units negative deviation from depleted mantle, "slightly enriched" values between 10 and 20 ε units negative deviation from depleted mantle, "enriched" values between ε units 20 and 30 negative deviation from depleted mantle, and "highly enriched" values >30 ε units negative deviation from depleted mantle. CHUR = bulk silicate Earth chonditic reservoir.

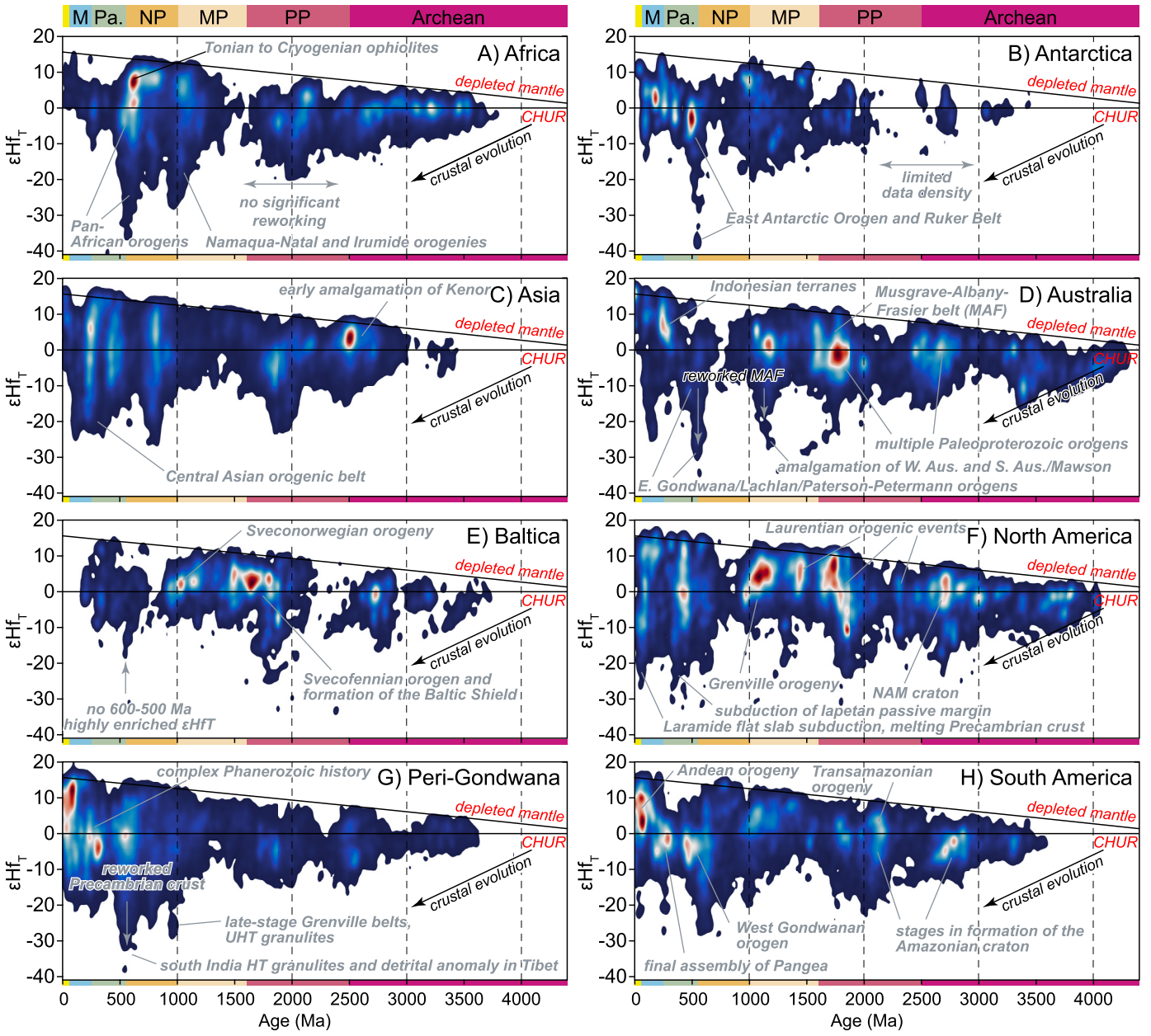

Fig. 4. Geographic and temporal distribution of εHf_T data by continental zone. A) Africa; B) Antarctica; C) Asia; D) Australia; E) Baltica; F) North America, G) Peri-Gondwana, H) South America. Bivariate KDEs were constructed with set kernel bandwidths of 20 Myr (x-axis) and 1 ε units (y-axis) using a modified version of *HafniumPlotter* (Sundell et al., 2019). Solid horizontal line is the bulk silicate Earth chonditic reservoir (CHUR).

Gondwana, and South America (Fig. 4A–B,G–H). Peri-Gondwana and South America show slightly enriched modes in the late Paleozoic to Mesozoic that transition into separate modes with depleted to slightly enriched εHf_T compositions (Fig. 4G–H). Africa, Antarctica, Australia, Peri-Gondwana, and South America, show a pronounced nadir at ~550 Ma, which includes highly enriched εHf_T values of nearly −40 (Fig. 4A–B,D,G–H). The Phanerozoic (541–0 Ma) shows a trend from enriched to more depleted εHf_T, with pronounced density modes in Antarctica, Peri-Gondwana, and South America (Fig. 4B,G–H).

Pairwise comparison of the eight continental zones results in twenty-eight plots that show where continental zones have similar εHf_T through time (Fig. 5). Bivariate KDEs are scaled relative to the maximum similarity of all twenty-eight density plots, which occurs in the late Neoproterozoic in the comparison between Antarctica and South America (Fig. 5W). In Fig. 5, warmer colors indicate where and when two continental zones share similar εHf_T. For example, the comparison between Africa and Antarctica shows two density modes, the first is depleted at ~1 Ga, and the second is slightly enriched to enriched at ~500 Ma (Fig. 5A), whereas there is limited similarity before 1 Ga (as shown by cooler colors or white space). Summing and normalizing the densities of all twenty-eight of the pairwise comparisons reveals five dominant density modes at ~2700, ~1800, ~1000, ~550, and ~300 Ma (Fig. 7A).

5. Discussion

5.1. Bias in the zircon Hf global record

The zircon εHf_T global record is geographically and temporally biased in terms of data density and Hf systematics (Figs. 2B, 3A–B,

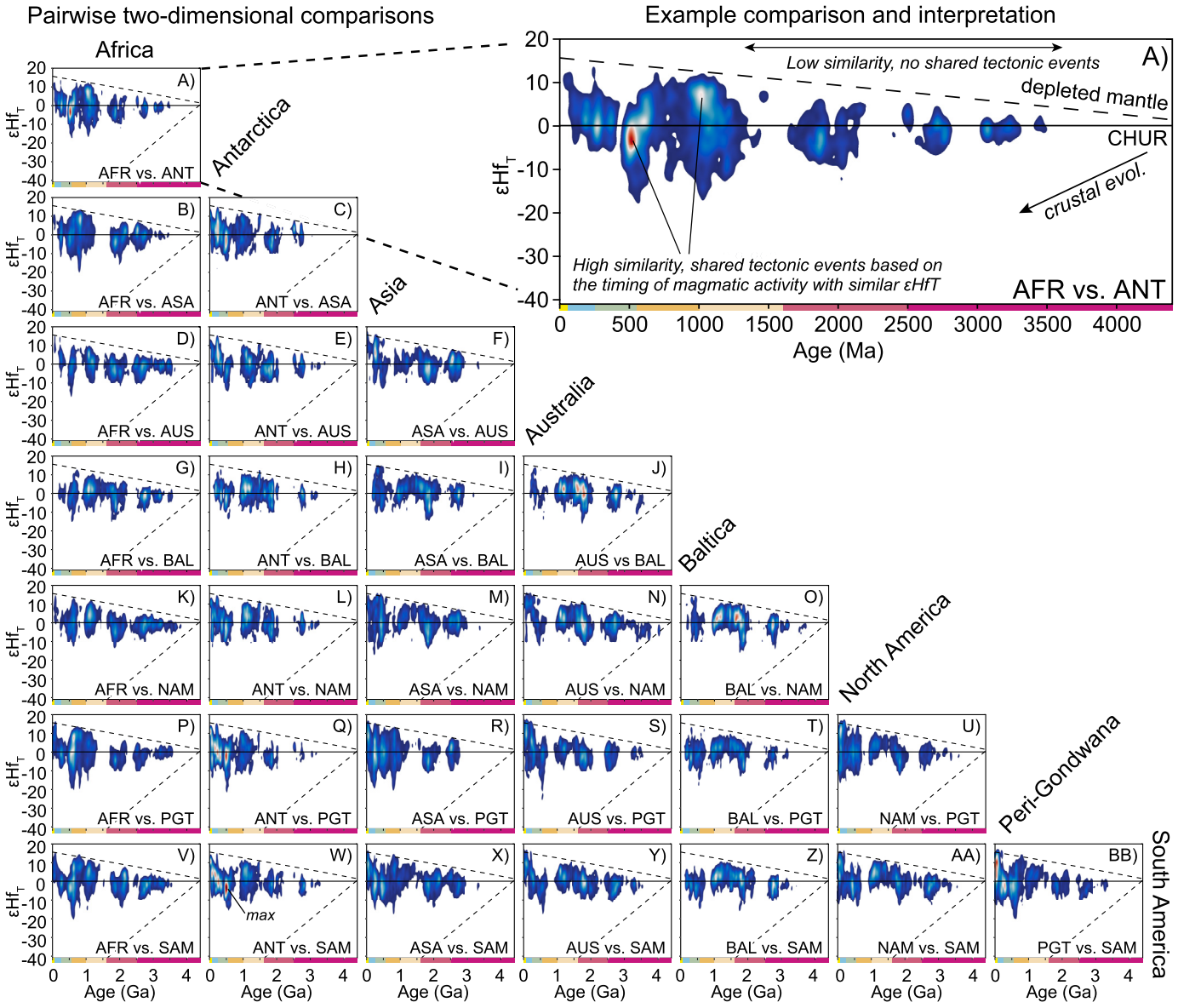

Fig. 5. Pairwise matrix of two-dimensional similarity between the eight continental zones calculated with a modified version of *DZstats2D* (Sundell and Saylor, 2021). Density modes represent where each pairwise comparison is similar (warm colors).

and Table 1). Geographically, the complete database shows the majority of data is concentrated in four areas, southern Asia, southern Africa, western Australia, and central Peri-Gondwana, in decreasing geographic data density (Fig. 2B). In fact, Asia and Peri-Gondwana data alone comprise ~48% of the total database (Table 1). Temporally, different continental zones dominate the global εHf_T record at different times. For example, the Hadean (>4000 Ma) is dominated by Australia, whereas the Archean is dominated by Africa, Asia, and South America (Fig. 3). The database has similarly divided contributions during the Neo- and Mesoproterozoic, which dramatically changes to dominance by Africa, Asia, Peri-Gondwana, and South America, followed by dominance by Asia, Peri-Gondwana, and South America in the Phanerozoic (Fig. 3). Such concentrations of data indicate there is significant temporal and geographic bias which can skew global scale interpretations of Earth processes when interpreted as a wholesale record.

Bias in the number of analyses as a fraction of the total database is due to partial preservation, more interior continental sampling compared to continental margins (Hawkesworth et al., 2009), and multi-cycle erosion and dispersal of detrital zircon. Because there is a bias to sample detrital rocks on continents with coherent stratigraphic context rather than in marginal basins that are modified by later tectonism, there is also a preservation and sampling bias towards zircon formed during continent-continent collisions that is preserved in interior basins (Fig. 1) (Hawkesworth et al., 2009). This bias reflects regional geological events that are weighted differently in the compiled record (Fig. 3A–B), in particular during widespread supercontinent assembly when specific εHf_T trends are more likely to be preserved and later sampled. Biases are inextricably linked in the global database because different geochemical signatures are produced in different orogenic events and orogenesis is variable in both space and time, which collectively results in different continental zones dominating parts of the global εHf_T record. As such, bias in the global database cannot be reduced by resampling methods (*e.g.*, via resampling inversely to data density, Keller et al., 2019), because such techniques merely enhance the under-sampled data temporally, and with no geographic or geologic context; such approaches inflate the relative

Table 1
Puetz et al. (2021) εHf_T Database Contributions.

			All	AFR	ANT	ASA	AUS	BAL	NAM	PGT	SAM
Igneous + Detrital	*n*	All	155329	24950	4020	44113	15197	5297	15343	30702	15707
		Depleted	70847	12709	1225	20564	7517	3121	8785	10407	6519
		Slightly Enriched	61211	8918	2248	15882	6494	1858	4860	13787	7164
		Enriched	18297	2447	478	5958	841	273	1419	5177	1704
		Highly Enriched	4974	876	69	1709	345	45	279	1331	320
	Database Fraction (%)	All	100.0	16.1	2.6	28.4	9.8	3.4	9.9	19.8	10.1
		Depleted	45.6	8.2	0.8	13.2	4.8	2.0	5.7	6.7	4.2
		Slightly Enriched	39.4	5.7	1.4	10.2	4.2	1.2	3.1	8.9	4.6
		Enriched	11.8	1.6	0.3	3.8	0.5	0.2	0.9	3.3	1.1
		Highly Enriched	3.2	0.6	0.0	1.1	0.2	0.0	0.2	0.9	0.2
Igneous	*n*	All	46809	4867	2078	14776	4624	2085	4199	10247	3933
		Depleted	22646	3070	721	7531	2664	1271	2606	3356	1427
		Slightly Enriched	17401	1140	1103	4879	1788	629	1158	4701	2003
		Enriched	5454	511	236	1685	147	155	405	1855	460
		Highly Enriched	1308	146	18	681	25	30	30	335	43
	Database Fraction (%)	All	30.1	3.1	1.3	9.5	3.0	1.3	2.7	6.6	2.5
		Depleted	14.6	2.0	0.5	4.8	1.7	0.8	1.7	2.2	0.9
		Slightly Enriched	11.2	0.7	0.7	3.1	1.2	0.4	0.7	3.0	1.3
		Enriched	3.5	0.3	0.2	1.1	0.1	0.1	0.3	1.2	0.3
		Highly Enriched	0.8	0.1	0.0	0.4	0.0	0.0	0.0	0.2	0.0
Detrital	*n*	All	108471	20083	1942	29302	10573	3212	11130	20455	11774
		Depleted	48197	9639	504	13029	4853	1850	6179	7051	5092
		Slightly Enriched	43789	7778	1145	10995	4706	1229	3689	9086	5161
		Enriched	12819	1936	242	4250	694	118	1013	3322	1244
		Highly Enriched	3666	730	51	1028	320	15	249	996	277
	Database Fraction (%)	All	69.8	12.9	1.3	18.9	6.8	2.1	7.2	13.2	7.6
		Depleted	31.0	6.2	0.3	8.4	3.1	1.2	4.0	4.5	3.3
		Slightly Enriched	28.2	5.0	0.7	7.1	3.0	0.8	2.4	5.8	3.3
		Enriched	8.3	1.2	0.2	2.7	0.4	0.1	0.7	2.1	0.8
		Highly Enriched	2.4	0.5	0.0	0.7	0.2	0.0	0.2	0.6	0.2

*Data from Puetz et al. (2021). AFR = Africa. ANT = Antactica. ASA = Asia. AUS = Australia. BAL = Baltica. NAM = North America. PGT = Peri-Gondwana. SAM = South America. Original data set contains $n = 165{,}111$, the data used for analysis ($n = 155{,}329$) excludes data outside the bounds of the continental zones as well as 'miscellaneous' type data from Puetz et al. (2021).

importance of gaps in global records by disproportionately weighting database outliers.

The global database is also biased in terms of εHf_T deviation from depleted mantle. An extreme example is the group of highly enriched zircon εHf_T data which is limited to ~3% of the global database (Table 1). Highly enriched zircon εHf_T data show further variability based on continental zone, with Africa, Asia, and Peri-Gondwana dominating the global record (Table 1). The implication here is that although the cratonic interiors indeed preserve the igneous record, that individual orogenic belts will produce zircon with εHf_T values that vary depending on the tectonic context. The Circum-Pacific is an example of external orogenesis that has produced dominantly depleted zircon εHf_T during the Cenozoic, whereas orogens of North and South China and the Himalaya are examples of internal orogenesis that produced a spread of depleted to highly enriched zircon εHf_T (Collins et al., 2011). Furthermore, temporally specific orogenic belts dominate the global database, which can be seen in each continental zone, for example, the prominent ~1100 Ma Grenville orogeny in North America (Fig. 4F).

Despite differing database contributions from igneous and detrital zircon εHf_T data, results show similar first order patterns for respective continental zones (Fig. 3). This similarity suggests that the detrital record is broadly representative of the preserved whole rock igneous record on billion-year timescales. Although sedimentary processes redistribute detrital zircons, especially where adjacent to a major orogenic belt or involved in collisional orogenesis, cratonic interiors reflect the magmatic signature of the orogens being weathering. However, the similarity between igneous and detrital εHf_T data does not hold true for shorter (i.e., 100 Myr) temporal intervals in the εHf_T database, which can be seen in the abundance of detrital zircon εHf_T data in Africa that is absent in the corresponding igneous record from 200 Ma to present (compare Figs. 3C and 3D). As such, the characteristics of a particular orogen, coupled with over- or under-sampling, produce anomalies on continents involved in collision resulting in density modes that are obfuscated by time-averaged trends in εHf_T, thus calling into question interpretations invoking global phenomena based on εHf_T archives (*e.g.*, Keller et al., 2019).

5.2. Tectonic interpretation of zircon Hf records

Bivariate KDEs of individual continental zones reveal patterns that can be interpreted in a plate tectonic context. In several cases, results show pulses of depleted εHf_T followed by crustal magmatism as documented by decreasing values through time such that εHf_T values evolve along a predictable crustal evolution line attributable to crustal reworking (*e.g.*, Figs. 3C, 4A). Vertical dispersion is likely due to mixing of depleted and enriched sources during generation of a melt within the crustal column as is common during crustal thickening and orogenesis, and especially common as orogenies terminate (*e.g.*, slab break-off, delamination, *etc.*). Below, we interpret the εHf_T records of each of the eight continental zones in the context of major orogenic events (Figs. 3–5).

5.2.1. Africa

Africa εHf_T data make up 16.1% of the zircon εHf_T database with major contributions (34% on average) at ~3600-2900 Ma, ~2200-2100 Ma, and ~1100–600 Ma; Africa contributes >50% of the global database at 3200–3100 Ma (Fig. 3A–B, Table 1). Results show that the Archean and Paleoproterozoic crust was not significantly reworked between 2000–1100 Ma (Fig. 4A). Crustal reworking took place between 1100 and 950 Ma during the Namaqua-Natal and Irumide orogens of modern southern Africa and the ~660–520 Ma Pan-African orogens (Fig. 4A), which culminated in the *ca.* 520 Ma formation of Gondwana (Goscombe et al., 2020). Both the Namaqua-Natal and the East African orogen included sig-

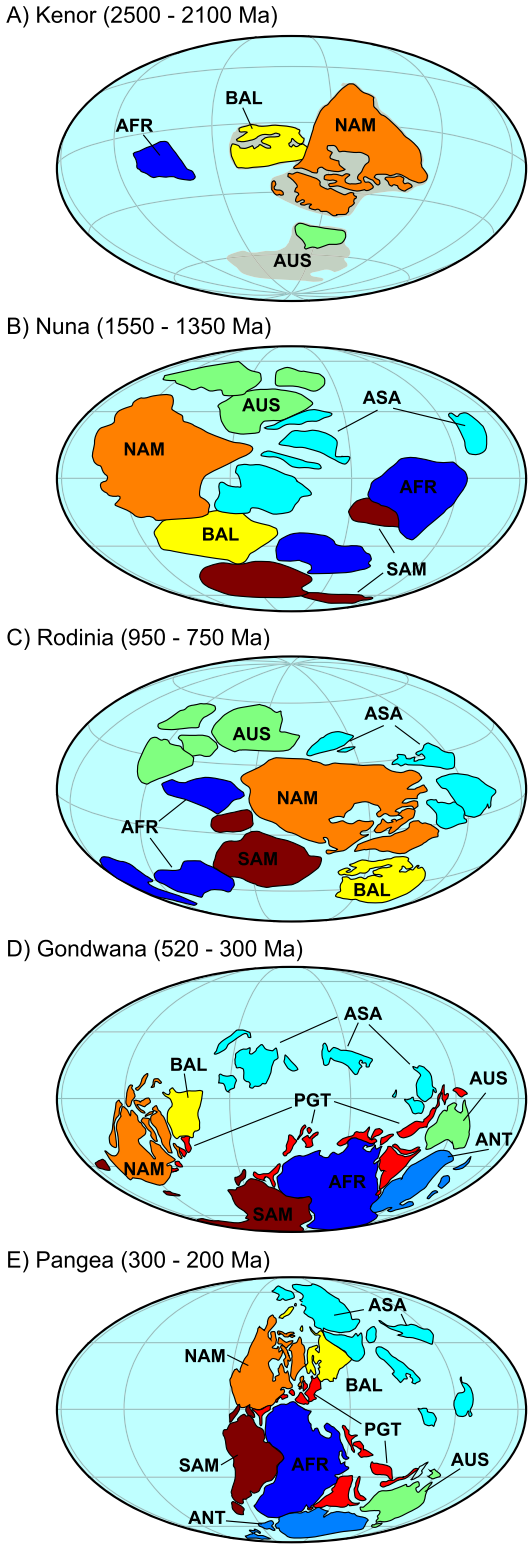

Fig. 6. Simplified paleogeographic reconstructions with supercontinent tenures based on Evans et al. (2016). A) Kenor at 2450 Ma (Pesonen et al., 2003). B) Nuna at 1400 Ma (Evans et al., 2016). C) Rodinia at 930 Ma (Ding et al., 2021). D) Gondwana at 410 Ma (Domeier and Torsvik, 2014). E) Pangea at 270 Ma (Domeier and Torsvik, 2014).

nificant depleted crustal addition (*e.g.*, Arabian-Nubian shield), the latter of which is marked by a large region of early to middle Neoproterozoic ophiolites and depleted melts (Johnson et al., 2011), as seen in a strong ~800–500 Ma depleted signal that accompanies the more highly enriched signal (Fig. 4A), and potentially reflects an interior versus peripheral orogenic signature (Collins et al., 2011). Highly enriched late Neoproterozoic εHf_T can be linked to the subduction of continental margins at ~600 Ma and reworking of pre-Neoproterozoic basement in the Borborema block and Nigerian shield as indicated by widespread ultra-high-pressure (UHP) metamorphism (Ganade de Araujo et al., 2014). After the Pan-African orogens, igneous activity in Africa was relatively quiet with slightly enriched to depleted values (Fig. 4A).

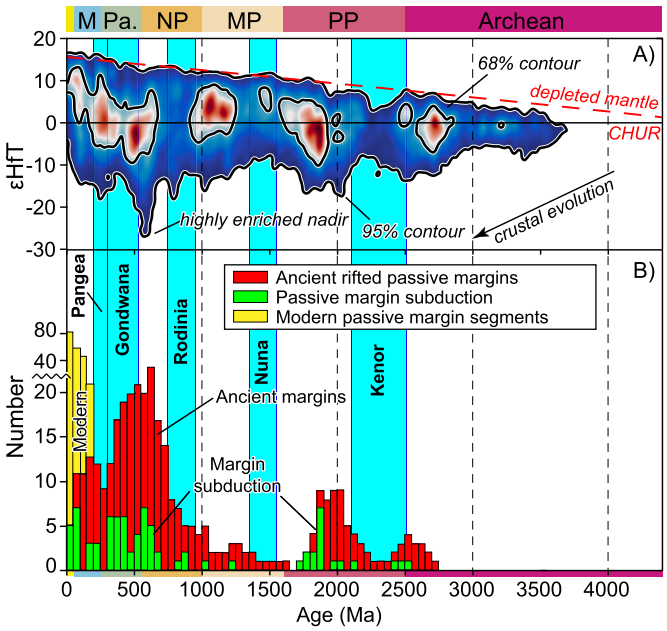

Fig. 7. Similarity sum compared to a compilation of passive margins. A) Similarity sum generated from adding the twenty-eight individual similarity comparisons shown in Fig. 5. Passive margin formation and destruction through Earth history (after Bradley, 2011).

5.2.2. Antarctica

Antarctica data are limited, making up only 2.6% of the zircon εHf_T database (Fig. 3A–B, Table 1). Despite the paucity of data, results show a particularly strong negative excursion to highly enriched Ediacaran-Cambrian values that we associate with the East Gondwana orogens between 600 and 500 Ma (Goscombe et al., 2020). These orogens reworked Archean and Proterozoic crust including ultra-high-temperature (UHT) granulites of the Mawson and Dharwar cratons in Antarctica and India, respectively, and the Napier complex of Antarctica (Goscombe et al., 2020).

5.2.3. Asia

Asia is the largest contributor to the zircon εHf_T database at 28.4% (Table 1), with an average contribution of ~30% from 2700–0 Ma (Fig. 3A–B). The Asia zircon εHf_T data show a ~2500 Ma pulse of depleted magmatism that can be linked to central Russia, Tarim, and eastern China, potentially associated with the early amalgamation of the Kenor supercontinent (Evans et al., 2016) (Fig. 4C). The ~1950 and 800 Ma events can be linked to orogenic events on Siberia, Tarim, North China, and Mongolia (*e.g.*, Bold et al., 2016). The dense array of *ca.* 400–100 Ma zircon εHf_T data is attributed to accretion and continent-continent collision in the Central Asian Orogenic Belt (Kröner et al., 2014).

5.2.4. Australia

Australia zircon εHf_T data make up 9.8% of the εHf_T database with major contributions from the Hadean and early Archean (4400–3900 Ma) and from ~1800–1100 (Fig. 3A–B, Table 1).

These data are consistent with significant crustal reworking by multiple Archean and Paleoproterozoic orogens at ~1800–1100 Ma (*e.g.*, Betts and Giles, 2006), resulting in a crustal evolution trend to more negative εHf_T through time (Fig. 4D). Depleted to slightly enriched εHf_T data at ~1600 Ma are the product of the primitive oceanic arc-backarc system that had enriched values in the Musgrave-Albany-Fraser belt that were subsequently reworked during the amalgamation of Western Australia and South Australia-Mawson at 1200 Ma (Smits et al., 2014), and then again during the late Neoproterozoic to early Paleozoic East Gondwana orogens (Goscombe et al., 2020). Highly enriched εHf_T values between 600–500 Ma developed in igneous sources in the Paterson-Petermann orogen and detrital sources associated with alluvial megafans that emerged from the Kuunga, Malagasy, and East Gondwana orogens (Squire et al., 2006). The final Cretaceous excursion to enriched εHf_T is limited to the Indonesian terranes and is related to the Cretaceous collision of the Argo and Banda terranes with the Malay Peninsula (Metcalfe, 2013) (Fig. 4D).

5.2.5. Baltica

Baltica, like Antactica, has limited data density with a contribution of only 3.4% (Fig. 3A–B, Table 1), but with a more sparse zircon εHf_T record that is mostly flat with depleted to slightly enriched values, with the exception of an excursion to enriched εHf_T values at ~1800 Ma (Fig. 4E). The excursion to enriched εHf_T values at ~1800 Ma marks the timing of the amalgamation of Archean crustal domains in the Svecofennian orogeny, which formed the Baltic Shield (Gorbatschev and Bogdanova, 1993). The major Mesoproterozoic magmatic pulse is associated with four-phase evolution of Fennoscandia in the 1200–900 Ma Sveconorwegian orogeny (Bingen et al., 2008) and progressively more negative εHf_T through time. Baltica does not preserve a late Neoproterozoic excursion to highly enriched values as shown in several other continental zones (Figs. 3–4). This is to be expected because by ~550 Ma Baltica had rifted away from Gondwana and Laurentia (Cocks and Torsvik, 2005), the Iapetus ocean had opened, and Baltica was isolated from the belts that were reworking old crust.

5.2.6. North America

North America zircon εHf_T data make up 9.9% of the εHf_T database, with an average global contribution of 25% at 4100–3600 Ma, 3100–2700 Ma, and 1800–1300 Ma (Fig. 3A–B). Pulses of Archean and Paleoproterozoic magmatism occurred during multiple collisional and accretionary orogens, the most intense of which producing depleted to slightly enriched magmatism related to the Paleoproterozoic assembly of Laurentia (Hoffman, 1988), including a large spread in values between ~1800–1700 Ma associated with the Trans-Hudson and Penokean belts (Hoffman, 1988). The ~1100 Ma signal associated with the Grenville orogen is depleted because it incorporated long-lived arc terranes and the arc-arc collision of two external orogens (Spencer et al., 2013). North America also shows major negative excursions at ~450 Ma and at ~50 Ma, related to the subduction of the Iapetan rifted passive margin in the Appalachian orogen, and to Laramide related partial melting of Archean–Proterozoic rocks (Stevens et al., 2016), respectively (Fig. 4F). Like Baltica, North America does not preserve a late Neoproterozoic excursion to enriched values because the Iapetus Ocean had already opened by that time and it was also isolated from Gondwanan orogenic belts (Cocks and Torsvik, 2005).

5.2.7. Peri-Gondwana

Peri-Gondwana zircon εHf_T data make up 19.8% of the zircon εHf_T database with an increasing contribution through time that is particularly dominant (30% on average) from 800-0 Ma (Fig. 3A–B, 4G, Table 1). The ~1000 Ma anomaly may be related to late-stage Rodinia-assembly belts including those in Africa, Antarctica, India, and Brazil (Hoffman, 1991), which host extensive UHT granulites (Korhonen et al., 2013). Melt extraction associated with UHT metamorphism of ancient continental crust is a mechanism to generate highly enriched εHf_T values in zircon (see Section 2). The excursion to negative εHf_T in the late Neoproterozoic can be linked to the southern tip of India where magmatism is associated with high T granulites in the intersection of the Kuunga-Malagasy orogen that united east and west Gondwana and extended into Antarctica and Madagascar (Goscombe et al., 2020).

5.2.8. South America

South America zircon εHf_T data make up 10.1% of the εHf_T database, with an average global contribution of 20% at 3000–2800 Ma, 2200–2100 Ma, and over the past ~100 Ma (Fig. 3A–B, Table 1). South American Neoarchean to Paleoproterozoic εHf_T values are depleted to slightly enriched during island arc accretion and early amalgamation of the central Amazon craton (Cordani et al., 2009) (Fig. 4H). The enriched 2200-2000 Ma εHf_T values are associated with the Transamazonian orogeny and final cratonization of the Amazon (Teixeira et al., 1989). Highly enriched Ediacaran-Cambrian detrital εHf_T values spread throughout southern Brazil, Argentina, and the southern Cordillera are related to Paleozoic and Mesozoic basins with West Gondwanan igneous sources (Squire et al., 2006). The slightly enriched to enriched 300–250 Ma εHf_T values are associated with basement gneisses that were intruded by Permian continental arc granites during the final assembly of Pangea in Mexico and the Northern Andes (Kirsch et al., 2012). A concentration of depleted Cenozoic εHf_T values is related to the recent and ongoing Cordilleran orogeny (Pepper et al., 2016).

5.3. Supercontinents

Below, results are discussed in the context of the five previously recognized supercontinents in Earth's history: Kenor, Nuna, Rodinia, Gondwana, and Pangea (Fig. 6). Importantly, we have defined supercontinent tenure based on paleomagnetic and geological data (Evans et al., 2016).

5.3.1. Kenor (2500–2100 Ma)

Kenor (a.k.a. Kenorland, Superia) formed by 2500 Ma and consisted of much of modern North America along with the Baltic Shield, the Kaapvaal craton of southern Africa, and the Pilbara craton of Australia (Pesonen et al., 2003) (Fig. 6A). Between 2700–2500 Ma, all of the continental zones show a high density of slightly enriched εHf_T values with a tail towards more enriched values, consistent with extensive crustal reworking during the formation of Kenor. Pairwise comparison highlights which zones were involved in the formation of Kenor. Similarity modes occur at ~2500 Ma involving comparisons of Asia, Australia, Baltica, and North America (Fig. 5F, J, O), as well as other early cratons suggested to not have been a part of Kenor (Pesonen et al., 2003), yet share similar εHf_T such as the Kalahari and Amazon cratons of Africa and South America (Figs. 5G,Z, 6A).

5.3.2. Nuna (1550–1350 Ma)

Nuna (*a.k.a.* Columbia, Hudsonland) formed progressively through the assembly of the United Plates of America (Hoffman, 1988), with Baltica and Siberia as its core and fragments of Africa, Australia, and South America on its periphery (Evans et al., 2016) (Fig. 6B). The negative εHf_T values at ~2000–1900 Ga in Asia and Africa slightly predate negative excursions at ~1800 Ga in Baltica and North America and at ~1700 Ma in Australia (Fig. 4), both of which are the result of the progressive assembly of Nuna. The similarity sum shows a mode between ~1800–1700 Ma associated with a spread in data (Fig. 7A). This feature corresponds with the final assembly of much of North America, which included

the Trans-Hudson and Penokean belts – the building blocks for Nuna (Hoffman, 1988). These orogens are analogous to the Pan-African belts and construction of Gondwana prior to joining with Laurussia to create Pangea (see below). Interestingly, pairwise comparison of bivariate KDEs highlights that Australia has significant similarity with Baltica and North America (Fig. 5J,N,O), despite its reconstructed geographic position being on the fringe of the supercontinent (Fig. 6B). A spread of 1800–1700 εHf_T values is also apparent in Australia's igneous record, suggesting that Australia experienced a coincident early construction before final emplacement in Nuna. This spread of 1800–1700 εHf_T values overlaps in time with collisions between the West Australian, North Australian, and Gawler cratons (Betts and Giles, 2006).

5.3.3. Rodinia (950–750 Ma)

Rodinia formed between ~1200–950 Ma through the assembly of continents along late Mesoproterozoic orogenic belts involving Antarctica, Australia, Kalahari, South America, Baltica, and North America (Fig. 6C) (Evans et al., 2016; Ding et al., 2021). The construction of Rodinia did not directly follow a full break-out of Nuna, as displayed by the low number of Mesoproterozoic rifted passive margins (Fig. 7) (Bradley, 2011). Instead, many of the orogenic belts involved in the construction of Rodinia contain long-lived arc terranes, such as the Grenville margin (Spencer et al., 2013), with extensive depleted crust formation that was reworked in the terminal collisions. Evidence for long-lived arcs is apparent in the late Mesoproterozoic εHf_T record from North America and Baltica (Fig. 4E–F), which shows abundant slightly enriched εHf_T values, but few highly enriched values, and is also shown in peaks in similarity of comparisons of Antarctica, Australia, Baltica, and North America, all of which have depleted εHf_T (Fig. 5H,J,L,N,O). This analysis is consistent with the hypothesis of Spencer et al. (2013) that Rodinia was assembled primarily through external orogenesis that reworked young crust.

5.3.4. Gondwana (520–300 Ma)

Gondwana involved the amalgamation of Africa, Antarctica, Australia, Peri-Gondwana, and South America. Final collision involved Africa with fragments of Australia and Antarctica to the east along the East African and Kuunga-Malagasy orogens, and suturing of Africa with South America to the west along the West Gondwana orogen (Fig. 6D, Goscombe et al., 2020); note that Gondwana's status as a supercontinent is contentious, see Evans et al. (2016) and Murphy et al. (2021) and references therein. Gondwanan sutures mark arc-continent and continent-continent collisions with extensive UHT granulite belts (Domeier and Torsvik, 2014) and widespread UHP metamorphism associated with the subduction of Neoproterozoic continental margins that formed on Archean to Proterozoic basement (*e.g.*, Ganade de Araujo et al., 2014). An important feature of the West Gondwana and Kuunga-Malagasy orogens is that many of the tectonic blocks involved in these collisions incorporated Tonian to Cryogneian (1000–635 Ma) rifted margins of Archean to Paleoproterozoic crust. The short lifespan of subducted passive continental margins (Fig. 7B) (Bradley, 2011) and the lack of significant Neoproterozoic depleted crust formation between these ancient continental margins resulted in more enriched melts compared to all other supercontinents (Fig. 4A,B,D,G,H). Maximum similarity occurs over a wide vertical range between slightly enriched and enriched εHf_T for continental zones involved in the formation of Gondwana, particularly highlighted by comparisons between Africa, Antarctica, Peri-Gondwana, and South America (Fig. 5A,C,P,Q,V,W,BB).

5.3.5. Pangea (300–200 Ma)

Pangea involved the amalgamation of most of the modern continental zones and formed by ~300 Ma with the final collision of Laurussia with Gondwana (Fig. 6E) (Domeier and Torsvik, 2014). However, only specific locations preserve similar εHf_T records, with depleted density modes at this time only occurring in Antarctica, Asia, Peri-Gondwana, and South America (Fig. 4B,C,F,G); peak similarity occurs in comparisons involving these continental zones (Fig. 5C,Q,W,X,BB). Although Australia and Antarctica were part of Pangea, they were far from the orogenic belts, and with the opening of the Atlantic Ocean these belts subsided which restricted transcontinental sediment dispersion.

5.4. Secular trends modulated by supercontinent formation and breakup

Major orogenic events in Earth's history govern secular trends of the global εHf_T. If zircon was evenly and efficiently extracted and sampled from old and young crust throughout Earth history, the global εHf_T plot would fan to a filled triangular array bounded at values of ~15 to ~−40 in the modern. Instead, there are gaps in the record with limited enriched values such as in the Mesoproterozoic and in the Mesozoic (Figs. 3–5).

The Mesoproterozoic experienced a lull in rifted passive margins and passive margin subduction via arc-continent collision, prompting the suggestion that Nuna transformed into Rodinia without a full supercontinent break-up (Fig. 7B) (Bradley, 2011). Gondwana produced the most enriched εHf_T in Earth's history and is followed by a return to more depleted εHf_T during Pangea amalgamation, because the major pieces of Pangea were assembled primarily during the formation of Gondwana (Fig. 6E–F), in a similar fashion to 1.8–1.7 Ga collisions that culminated in the supercontinent of Nuna. The Cenozoic trend in global similarity (Fig. 7A) is driven largely by depleted melts in Peri-Gondwana terranes and highlights the importance of where melt is being extracted, such as Himalayan melts being extracted from Tethyan island arc terranes. The depleted trends in the Mesoproterozoic and Mesozoic to present are coincident with lulls in passive margin subduction associated with collisional orogens (Fig. 7) (Bradley, 2011). During the Mesoproterozoic and Mesozoic, zircon was produced primarily in marginal arcs peripheral to Archean and Paleoproterozoic crust where, without full supercontinent breakup and generation of rifted passive margins, old continental crust was sequestered in continental interiors and inaccessible to major melt extraction (Fig. 7) (Collins et al., 2011).

The εHf_T similarity sum (Fig. 7A) highlights where common trends occur globally, with density modes that broadly predate the timing of supercontinent tenures of Kenor (2500–2100 Ma), Nuna (1550–1350 Ma), Rodinia (950–750 Ma), Gondwana (520–300 Ma), and Pangea (300–200 Ma) (Evans et al., 2016) (Fig. 7). We interpret these similarity modes to reflect abundant zircon generated in granites during arc-continent and continent-continent collisions that culminate in supercontinent formation. Zircon that crystallized in plutons formed in internal orogens during supercontinent assembly was later exhumed and distributed in intercontinental basins and margins during supercontinent tenure, resulting in shared patterns between adjoined cratons. We suggest that zircon abundance and similarity is highest during supercontinent assembly and decreases through supercontinent tenure (Fig. 7). During supercontinent tenure and break-up, new zircon generated in marginal arcs and external orogens that are not efficiently spread to adjacent continents and are less likely to be transported into continental interiors, resulting in lower similarity. Although complications arise due to localized phenomena such as flat-slab subduction or collisions in multiple disparate localities that generate melts with similar isotopic compositions at similar times, supercontinent formation remains a dominant force in producing shared geochemical histories in the preserved zircon εHf_T record.

6. Conclusions

Quantitative comparison of bivariate KDEs with geographic context provides a new way to evaluate similarity in zircon εHf_T between continental zones and highlights the role of specific tectonic processes that imprint the zircon εHf_T record. Results presented here support the interpretation that positive or negative excursions in global records of zircon εHf_T correspond to specific orogenic events associated with supercontinent amalgamation and separation and are not related to extreme erosion during Snowball Earth or secular changes in plate tectonics. Enriched εHf_T is the predicted product of Gondwana following rifting of Rodinia, which formed new passive continental margins on old radiogenic crust. On the other hand, Rodinia and Pangea produced depleted to slightly enriched εHfT as they were dominated by external orogenesis. The global εHf_T record contains geographic and temporal variation in the contributions of different continental zones through time. This same variation works to bias global interpretations when the database is interpreted without geographic context, and should not be reduced by resampling methods, as such techniques inappropriately augment data density gaps in the global record by disproportionately weighting inherent outliers.

CRediT authorship contribution statement

KES and FAM participated in the conceptualization, methodology, validation, data curation, writing, reviewing, and editing of this manuscript.

Declaration of competing interest

The authors declare that they have no known competing financial interests or personal relationships that could have appeared to influence the work reported in this paper.

Acknowledgements

We thank Steve Puetz for compiling and sharing the global hafnium database and all who made their data available. Reviews by Brendan Murphy, Christopher Hawkesworth, and Christopher Spencer greatly improved the quality and clarity of this work. We thank Editor Alexander Webb for handling of the manuscript. Peter Cawood, Kent Condie, Joshua Garber, Michael Hartnady provided valuable feedback on earlier versions of this work. This work was partially supported by the National Science Foundation grant EAR-1649254 to the Arizona LaserChron Center in support of KES and grants EAR-1759200, EAR-1926001, and EAR-1916698 to FAM.

Appendix A. Supplementary material

Supplementary material related to this article can be found online at https://doi.org/10.1016/j.epsl.2022.117426. MATLAB scripts and data used to generate the figures in this paper can also be found at github.com/kurtsundell/Global_Hf.

References

Ahmed, N., Natarajan, T., Rao, K.R., 1974. Discrete cosine transform. IEEE Trans. Comput. 100 (1), 90–93.
Andersen, T., 2014. The detrital zircon record: supercontinents, parallel evolution—or coincidence? Precambrian Res. 244, 279–287.
Andersen, T., Kristoffersen, M., Elburg, M.A., 2018. Visualizing, interpreting and comparing detrital zircon age and Hf isotope data in basin analysis–a graphical approach. Basin Res. 30 (1), 132–147.
Bea, F., 1996. Residence of REE, Y, Th and U in granites and crustal protoliths; implications for the chemistry of crustal melts. J. Petrol. 37 (3), 521–552.
Belousova, E.A., Kostitsyn, Y.A., Griffin, W.L., Begg, G.C., O'Reilly, S.Y., Pearson, N.J., 2010. The growth of the continental crust: constraints from zircon Hf-isotope data. Lithos 119 (3–4), 457–466.
Betts, P.G., Giles, D., 2006. The 1800–1100 Ma tectonic evolution of Australia. Precambrian Res. 144 (1–2), 92–125.
Bhattacharyya, A., 1943. On a measure of divergence between two statistical populations 661 defined by their probability distributions. Bull. Calcutta Math. Soc. 35, 99–109.
Bingen, B., Nordgulen, O., Viola, G., 2008. A four-phase model for the Sveconorwegian orogeny, SW Scandinavia. Nor. Geol. Tidsskr. 88 (1), 43.
Bold, U., Crowley, J.L., Smith, E.F., Sambuu, O., Macdonald, F.A., 2016. Neoproterozoic to early Paleozoic tectonic evolution of the Zavkhan terrane of Mongolia: implications for continental growth in the Central Asian orogenic belt. Lithosphere 8 (6), 729–750.
Bradley, D.C., 2011. Secular trends in the geologic record and the supercontinent cycle. Earth-Sci. Rev. 108 (1–2), 16–33.
Cocks, L.R.M., Torsvik, T.H., 2005. Baltica from the late Precambrian to mid-Palaeozoic times: the gain and loss of a terrane's identity. Earth-Sci. Rev. 72 (1–2), 39–66.
Collins, W.J., Belousova, E.A., Kemp, A.I., Murphy, J.B., 2011. Two contrasting Phanerozoic orogenic systems revealed by hafnium isotope data. Nat. Geosci. 4 (5), 333–337.
Condie, K.C., Bickford, M.E., Aster, R.C., Belousova, E., Scholl, D.W., 2011. Episodic zircon ages, Hf isotopic composition, and the preservation rate of continental crust. Bulletin 123 (5–6), 951–957.
Cordani, U.G., Teixeira, W., D'Agrella-Filho, M.S., Trindade, R.I., 2009. The position of the Amazonian Craton in supercontinents. Gondwana Res. 15 (3–4), 396–407.
Dhuime, B., Hawkesworth, C.J., Cawood, P.A., Storey, C.D., 2012. A change in the geodynamics of continental growth 3 billion years ago. Science 335 (6074), 1334–1336.
Ding, J., Zhang, S., Evans, D.A., Yang, T., Li, H., Wu, H., Chen, J., 2021. North China craton: the conjugate margin for northwestern Laurentia in Rodinia. Geology.
Domeier, M., Torsvik, T.H., 2014. Plate tectonics in the late Paleozoic. Geosci. Front. 5 (3), 303–350.
Evans, D.A.D., Li, Z.X., Murphy, J.B., 2016. Four-dimensional context of Earth's supercontinents. Geol. Soc. (Lond.) Spec. Publ. 424 (1), 1–14.
Ganade de Araujo, C.E.G., Rubatto, D., Hermann, J., Cordani, U.G., Caby, R., Basei, M.A., 2014. Ediacaran 2,500-km-long synchronous deep continental subduction in the West Gondwana Orogen. Nat. Commun. 5 (1), 1–8.
Gorbatschev, R., Bogdanova, S., 1993. Frontiers in the Baltic shield. Precambrian Res. 64 (1–4), 3–21.
Goscombe, B., Foster, D.A., Gray, D., Wade, B., 2020. Assembly of central Gondwana along the Zambezi Belt: metamorphic response and basement reactivation during the Kuunga Orogeny. Gondwana Res. 80, 410–465.
Griffin, W.L., Pearson, N.J., Belousova, E., Jackson, S.V., Van Achterbergh, E., O'Reilly, S.Y., Shee, S.R., 2000. The Hf isotope composition of cratonic mantle: LAM-MC-ICPMS analysis of zircon megacrysts in kimberlites. Geochim. Cosmochim. Acta 64 (1), 133–147.
Hawkesworth, C., Cawood, P., Kemp, T., Storey, C., Dhuime, B., 2009. A matter of preservation. Science 323 (5910), 49–50.
Hoffman, P.F., 1988. United plates of America, the birth of a craton: early proterozoic assembly and growth of Laurentia. Annu. Rev. Earth Planet. Sci. 16 (1), 543–603.
Hoffman, P.F., 1991. Did the breakout of Laurentia turn Gondwanaland inside-out? Science 252 (5011), 1409–1412.
Hofmann, A.W., 1997. Mantle geochemistry: the message from oceanic volcanism. Nature 385 (6613), 219–229.
Johnson, P.R., Andresen, A., Collins, A.S., Fowler, A.R., Fritz, H., Ghebreab, W., Kusky, T., Stern, R.J., 2011. Late Cryogenian–Ediacaran history of the Arabian–Nubian Shield: a review of depositional, plutonic, structural, and tectonic events in the closing stages of the northern East African Orogen. J. Afr. Earth Sci. 61 (3), 167–232.
Keller, C.B., Husson, J.M., Mitchell, R.N., Bottke, W.F., Gernon, T.M., Boehnke, P., Bell, E.A., Swanson-Hysell, N.L., Peters, S.E., 2019. Neoproterozoic glacial origin of the Great Unconformity. Proc. Natl. Acad. Sci. 116 (4), 1136–1145.
Kirsch, M., Keppie, J.D., Murphy, J.B., Solari, L.A., 2012. Permian–Carboniferous arc magmatism and basin evolution along the western margin of Pangea: geochemical and geochronological evidence from the eastern Acatlán Complex, southern Mexico. Bulletin 124 (9–10), 1607–1628.
Korhonen, F.J., Brown, M., Clark, C., Bhattacharya, S., 2013. Osumilite–melt interactions in ultrahigh temperature granulites: phase equilibria modelling and implications for the P–T–t evolution of the Eastern Ghats Province, India. J. Metamorph. Geol. 31 (8), 881–907.
Kröner, A., Kovach, V., Belousova, E., Hegner, E., Armstrong, R., Dolgopolova, A., Seltmann, R., Alexeiev, D.V., Hoffmann, J.E., Wong, J., Sun, M., 2014. Reassessment of continental growth during the accretionary history of the Central Asian Orogenic Belt. Gondwana Res. 25 (1), 103–125.
Metcalfe, I., 2013. Gondwana dispersion and Asian accretion: tectonic and palaeogeographic evolution of eastern Tethys. J. Asian Earth Sci. 66, 1–33.
Murphy, J.B., Nance, R.D., Cawood, P.A., Collins, W.J., Dan, W., Doucet, L.S., Heron, P.J., Li, Z.X., Mitchell, R.N., Pisarevsky, S., Pufahl, P.K., 2021. Pannotia: in defense of its existence and geodynamic significance. Geol. Soc. (Lond.) Spec. Publ. 503 (1), 13–39.

Patchett, P.J., White, W.M., Feldmann, H., Kielinczuk, S., Hofmann, A.W., 1984. Hafnium/rare Earth element fractionation in the sedimentary system and crustal recycling into the Earth's mantle. Earth Planet. Sci. Lett. 69 (2), 365–378.
Pepper, M., Gehrels, G., Pullen, A., Ibanez-Mejia, M., Ward, K.M., Kapp, P., 2016. Magmatic history and crustal genesis of western South America: constraints from U-Pb ages and Hf isotopes of detrital zircons in modern rivers. Geosphere 12 (5), 1532–1555.
Pesonen, L.J., Elming, S.Å, Mertanen, S., Pisarevsky, S., D'Agrella-Filho, M.S., Meert, J.G., Schmidt, P.W., Abrahamsen, N., Bylund, G., 2003. Palaeomagnetic configuration of continents during the Proterozoic. Tectonophysics 375 (1–4), 289–324.
Puetz, S.J., Spencer, C.J., Ganade, C.E., 2021. Analyses from a validated global UPb detrital zircon database: enhanced methods for filtering discordant UPb zircon analyses and optimizing crystallization age estimates. Earth-Sci. Rev. 220, 103745.
Roberts, N.M., Spencer, C.J., 2015. The zircon archive of continent formation through time. Geol. Soc. (Lond.) Spec. Publ. 389 (1), 197–225.
Schoene, B., 2014. U-Th-Pb geochronology. In: Holland, H.D., Turekian, K.K. (Eds.), Treatise on Geochemistry, second edition. Elsevier, Oxford, pp. 341–378.
Smits, R.G., Collins, W.J., Hand, M., Dutch, R., Payne, J., 2014. A Proterozoic Wilson cycle identified by Hf isotopes in central Australia: implications for the assembly of Proterozoic Australia and Rodinia. Geology 42 (3), 231–234.
Sobolev, S.V., Brown, M., 2019. Surface erosion events controlled the evolution of plate tectonics on Earth. Nature 570 (7759), 52–57.
Söderlund, U., Patchett, P.J., Vervoort, J.D., Isachsen, C.E., 2004. The 176Lu decay constant determined by Lu–Hf and U–Pb isotope systematics of Precambrian mafic intrusions. Earth Planet. Sci. Lett. 219 (3–4), 311–324.
Spencer, C.J., Hawkesworth, C., Cawood, P.A., Dhuime, B., 2013. Not all supercontinents are created equal: Gondwana-Rodinia case study. Geology 41 (7), 795–798.
Spencer, C.J., Dyck, B., Mottram, C.M., Roberts, N.M., Yao, W.H., Martin, E.L., 2019. Deconvolving the pre-Himalayan Indian margin–tales of crustal growth and destruction. Geosci. Front. 10 (3), 863–872.
Squire, R.J., Campbell, I.H., Allen, C.M., Wilson, C.J., 2006. Did the Transgondwanan Supermountain trigger the explosive radiation of animals on Earth? Earth Planet. Sci. Lett. 250 (1–2), 116–133.
Stevens, A.L., Balgord, E.A., Carrapa, B., 2016. Revised exhumation history of the Wind River Range, WY, and implications for Laramide tectonics. Tectonics 35 (5), 1121–1136.
Sundell, K., Saylor, J.E., Pecha, M., 2019. Provenance and recycling of detrital zircons from Cenozoic Altiplano strata and the crustal evolution of western South America from combined U-Pb and Lu-Hf isotopic analysis. In: Folguera, A., Horton, B.K. (Eds.), Andean Tectonics. Elsevier, pp. 363–397.
Sundell, K.E., Saylor, J.E., 2021. Two-dimensional quantitative comparison of density distributions in detrital geochronology and geochemistry. Geochem. Geophys. Geosyst. 22 (4), e2020GC009559.
Teixeira, W., Tassinari, C.C.G., Cordani, U.G., Kawashita, K., 1989. A review of the geochronology of the Amazonian Craton: tectonic implications. Precambrian Res. 42 (3–4), 213–227.
Thyng, K.M., Greene, C.A., Hetland, R.D., Zimmerle, H.M., DiMarco, S.F., 2016. True colors of oceanography: guidelines for effective and accurate colormap selection. Oceanography 29 (3), 9–13.
Vervoort, J.D., Blichert-Toft, J., 1999. Evolution of the depleted mantle: Hf isotope evidence from juvenile rocks through time. Geochim. Cosmochim. Acta 63 (3–4), 533–556.